nature communications

Article

https://doi.org/10.1038/s41467-025-57203-z

Translational error in mice increases with ageing in an organ-dependent manner

Received: 10 June 2024

Accepted: 10 February 2025

Published online: 28 February 2025

Check for updates

Erik C. Böttger[1], Harshitha Santhosh Kumar[1], Adrian Steiner[2], Emmanuel Sotirakis[3], Kader Thiam[3], Patricia Isnard Petit[3], Petra Seebeck[4], David P. Wolfer[2], Dimitri Shcherbakov[1,2,6] & Rashid Akbergenov[1,5,6]

The accuracy of protein synthesis and its relation to ageing has been of long-standing interest. To study whether spontaneous changes in the rate of ribosomal error occur as a function of age, we first determined that stop-codon readthrough is a more sensitive read-out of mistranslation due to codon-anticodon mispairing than missense amino acid incorporation. Subsequently, we developed knock-in mice for in-vivo detection of stop-codon readthrough using a gain-of-function Kat2-TGA-Fluc readthrough reporter which combines fluorescent and sensitive bioluminescent imaging techniques. We followed expression of reporter proteins in-vivo over time, and assessed Kat2 and Fluc expression in tissue extracts and by whole organ ex-vivo imaging. Collectively, our results provide evidence for an organ-dependent, age-related increase in translational error: stop-codon readthrough increases with age in muscle (+ 75%, $p < 0.001$) and brain (+ 50%, $p < 0.01$), but not in liver ($p > 0.5$). Together with recent data demonstrating premature ageing in mice with an error-prone *ram* mutation, our findings highlight age-related decline of translation fidelity as a possible contributor to ageing.

Being the endpoint of the implementation of genetic information, the ability to accurately translate nucleic acids into functional proteins is central for all living organisms. Reportedly, errors in DNA replication occur at a frequency of 10^{-8}–10^{-9} and the error rate in mRNA transcription is in the range of 10^{-6} [1,2]. By comparison, the average error rate in mRNA decoding by the ribosome has been estimated to be in the range of 10^{-4} per codon, making it the limiting factor in the accuracy of gene expression[3]. The rare errors in mRNA decoding by the ribosome mostly result from codon-anticodon mispairings as per accommodation of mismatched aa-tRNAs[4–6], such as missense substitutions or stop-codon readthrough[3,7]. Due to the physical constraints of the mRNA-tRNA interaction, accommodation of mismatched tRNAs in the ribosomal decoding A-site is limited to near-cognate tRNAs[8,9]. As a result, missense amino acid substitutions are mostly conservative in nature because of the way the genetic code is arranged[10]. Stop-codon readthrough occurs when a ribosome positioned with a stop codon in the A-site incorporates an amino acid into the nascent polypeptide chain, instead of terminating translation by hydrolysis and release of the polypeptide from the P-site peptidyl-tRNA, a process mediated by binding of eukaryotic release factor 1 directly recognizing the three stop codons UGA, UAG, and UAA. The frequency of insertion of individual missense amino acids is distinct for different stop codons[11].

Ribosomal errors are codon and sequence dependent, and affected by both ribosomal and non-ribosomal mechanisms, e.g., post-transcriptional modifications of RNA (rRNA, tRNA, mRNA)[12–16], abundance and posttranslational modifications of ribosomal proteins and translation factors[17,18], and levels and accuracy of tRNA aminoacylation[19,20]. Back in the 1980s, attempts were undertaken to investigate whether translational accuracy in mammalians declines

[1]Institut für Medizinische Mikrobiologie, Universität Zürich, Zurich, Switzerland. [2]Anatomisches Institut, Universität Zürich, and Institut für Bewegungswissenschaften und Sport, ETH Zürich, Zurich, Switzerland. [3]genOway, F-69362, Lyon, France. [4]Zurich Integrative Rodent Physiology (ZIRP), University of Zurich, Zurich, Switzerland. [5]Biozentrum University of Basel, Basel, Switzerland. [6]These authors contributed equally: Dimitri Shcherbakov, Rashid Akbergenov. e-mail: rashid.akbergenov@unibas.ch

with organismal or cellular aging, mainly using human diploid fibroblasts or ribosomal extracts from rodent liver. With the exception of a single report in late stage human fibroblasts measuring misincorporation of [^{35}S] -cysteine into a viral protein lacking any codon for cysteine[21], all of the other studies conducted at that time were unable to show an age-associated increase in mistranslation[22–30], for recent review see ref. 31. However, it was noted that there are important caveats limiting these early studies. Many of them were conducted in-vitro with isolated ribosomes, which may or may not recapitulate the many extra-ribosomal factors which contribute to in-vivo translation accuracy. In addition, the assays used to record mistranslation in the 1980s used either highly artificial translation substrates, such as poly-U, or had insufficient sensitivity to reliably detect those rare aberrant proteins due to ribosomal error, such as analysis of proteins on 2D gels[21,32,33].

More recent work points to translation as an emerging constraint on protein homeostasis in aging, indicating that complex age-associated changes may affect ribosome function, including decreased translation elongation, decoupling of transcription and translation, and loss of ribosome stoichiometry due to age-related decline in proteasome activity[34–36], for review see ref. 37. Specifically, recent studies have implicated translational fidelity as an important determinant of lifespan. Thus, translational accuracy has been suggested to positively correlate with maximum possible life span among different rodent species indicating a possible link between translational accuracy, life span, and potentially age-accelerating effects of translational error[38]. This perception is supported by the recent demonstration that by experimentally increasing the fidelity of protein synthesis the life span in yeast and non-mammalian metazoans can be extended[39]. Conversely, experimentally increasing the ribosomal error rate in mice by generation of knock-in mice which carry the RPS9 D95N ram (ribosomal ambiguity) mutation was found to result in premature ageing and shortened life span[40].

To study translational fidelity in mammalians in-vivo and to address the question whether spontaneous changes in the rate of misreading occur as a function of age we here developed modified versions of highly sensitive gain-of-function dual reporter constructs which express firefly luciferase (Fluc) fusion proteins. Following demonstration of stop-codon readthrough as the most sensitive readout of codon-anticodon mispairing, we generated knock-in mice which carry the dual reporter readthrough construct Kat2-TGA-Fluc. This reporter combines fluorescence with bioluminescence measurements and is suitable for real-time non-invasive in-vivo imaging, ex-vivo whole organ imaging, and detailed analysis of reporter expression in tissue extracts. Using these mice, we recorded expression of the reporter proteins in live animals in-vivo over time, followed by whole organ ex-vivo imaging and measurement of reporter activities in tissue extracts. We found that stop-codon readthrough increases with age in an organ-dependent manner. Together with the recent observation that heightened levels of translational error result in premature ageing and development of age-related diseases[40–42], our findings reported here point to the possibility that an age-associated increase in translational error as recorded by stop-codon readthrough and as observed primarily in postmitotic tissues (brain, muscle) may be an important contributor to the overall ageing process and the age-related decline in protein homeostasis.

Results

Choice of reporters

We used dual luciferase reporters[42,43] to quantitatively assess the error frequency of two types of codon-anticodon mispairing: accommodation of near-cognate aa-tRNAs at a sense codon resulting in missense misreading, and accommodation of aa-tRNAs at a stop codon resulting in stop-codon readthrough (Fig. 1). In dual luciferase reporters a humanized Renilla luciferase (hRluc)−Firefly luciferase (hFluc) fusion protein, separated by a linker, is produced. Rluc serves as measure for total translation of the reporter, while Fluc reports missense miscoding or stop-codon readthrough. To record missense miscoding, H245^{CAC} in the active site of Fluc was mutated to near-cognate R245^{CGC}, resulting in enzymatically nonfunctional Fluc; to record readthrough D357 of Fluc was mutated from GAC to stop codon TAG or TGA, producing a truncated protein devoid of Fluc activity[42]. Fluc activity is regained by missense miscoding at 245^{CGC} or stop codon readthrough at 357$^{TGA/TAG}$, respectively. For validation of the misreading reporters we used the aminoglycoside geneticin, a well-established mistranslation-inducing agent[44] and ribosomes with the *RPS9^{D95N} ram* mutation[41] as positive controls.

HEK293 cells expressing wild-type *RPS9^{WT}* or mutant *RPS9^{D95N}* [41] were transfected with the dual luciferase reporter constructs. For quantitation of absolute levels of misreading and readthrough, HEK293 WT cells were in parallel transfected with construct pRM Rluc-Fluc WT. Absolute mistranslation values were calculated by the ratio of Fluc^{CGC}/Rluc to Fluc^{WT}/Rluc for misreading and Fluc^{TAG}/Rluc or Fluc^{TGA}/Rluc to Fluc^{WT}/Rluc for readthrough on TAG or TGA stop codons, respectively. Frequency of missense translation errors in HEK293 WT cells was determined as $3.4 \pm 0.3 \times 10^{-4}$. Readthrough errors occurred with a frequency of $4.03 \pm 0.13 \times 10^{-3}$ on TGA codon and $1.82 \pm 0.12 \times 10^{-3}$ on TAG codon (Table 1 and Suppl. Fig. 1). As reported previously[41], *RPS9^{D95N}* mutant cells showed increased levels of near-cognate misreading (twofold) and TGA stop codon readthrough (sevenfold), compared to *RPS9^{WT}* (Fig. 1). Treatment of *RPS9^{WT}* cells with geneticin induced both CGC misreading and TGA readthrough errors in a dose-dependent manner. Readthrough on TAG codon showed less induction both by the *RPS9^{D95N}* mutation and upon geneticin treatment of *RPS9^{WT}* cells, as compared to readthrough on the TGA stop codon (Table 1 and Fig. 1A–C). These results are in line with previous investigations[11], which found that UGA is more permissive than UAG for stop-codon readthrough.

Together, these results demonstrate that readthrough of TGA stop codons is the most sensitive readout of ribosomal mistranslation due to codon-anticodon mispairing.

Dual luciferase reporters are commonly used to study ribosomal mistranslation in-vitro and in cell cultures. The two different luciferases, Rluc and Fluc, utilize different substrates, which are added sequentially, as the signal of the first substrate must be quenched to allow for measuring the signal generated by the second substrate. While this methodology is convenient for analysis of cell cultures or in-vitro translation experiments, it poses problems for in-vivo assessments of translation fidelity. The need for two different substrates, applied sequentially, together with the requirement for complete signal quenching, makes dual luciferase reporters unsuitable for in-vivo measurements. For in-vivo monitoring of translation fidelity, a preferable option is to use reporter constructs which combine the highly sensitive Fluc bioluminescent readout with a fluorescent reporter, the latter used for normalization of reporter translation[45]. Accordingly, we replaced Rluc in vector pRM hRluc-hFlucWT with the fluorescent reporter Katushka2S (Kat2) and introduced a TGA stop codon into the linker which separates Kat2 and Fluc, resulting in the stop-codon readthrough reporter Kat2-TGA-Fluc (Fig. 1A). Katushka is a far-red fluorescent protein, which spectrum does not interfere with firefly luciferase, and which can be fused with Fluc luciferase without losing activity[45]. Katushka2S was chosen as fluorescent reporter, as it exhibits higher brightness, faster maturation and superior signal-to-noise ratio compared to Katushka and other far-red fluorescent proteins[46].

We first validated the Kat2-TGA-Fluc reporter by functional measurements in transfected HEK cells treated with geneticin. Relative readthrough values were calculated by the ratio of Fluc^{TGA}/Kat2. As expected, we found that treatment with geneticin induced TGA readthrough in a dose-dependent manner, up to 13-fold at 400 μM (Fig. 1D). Control Kat2-Fluc transfected cells encoding an uninterrupted Kat2-Fluc fusion protein showed no Fluc induction by geneticin,

https://doi.org/10.1038/s41467-025-57203-z

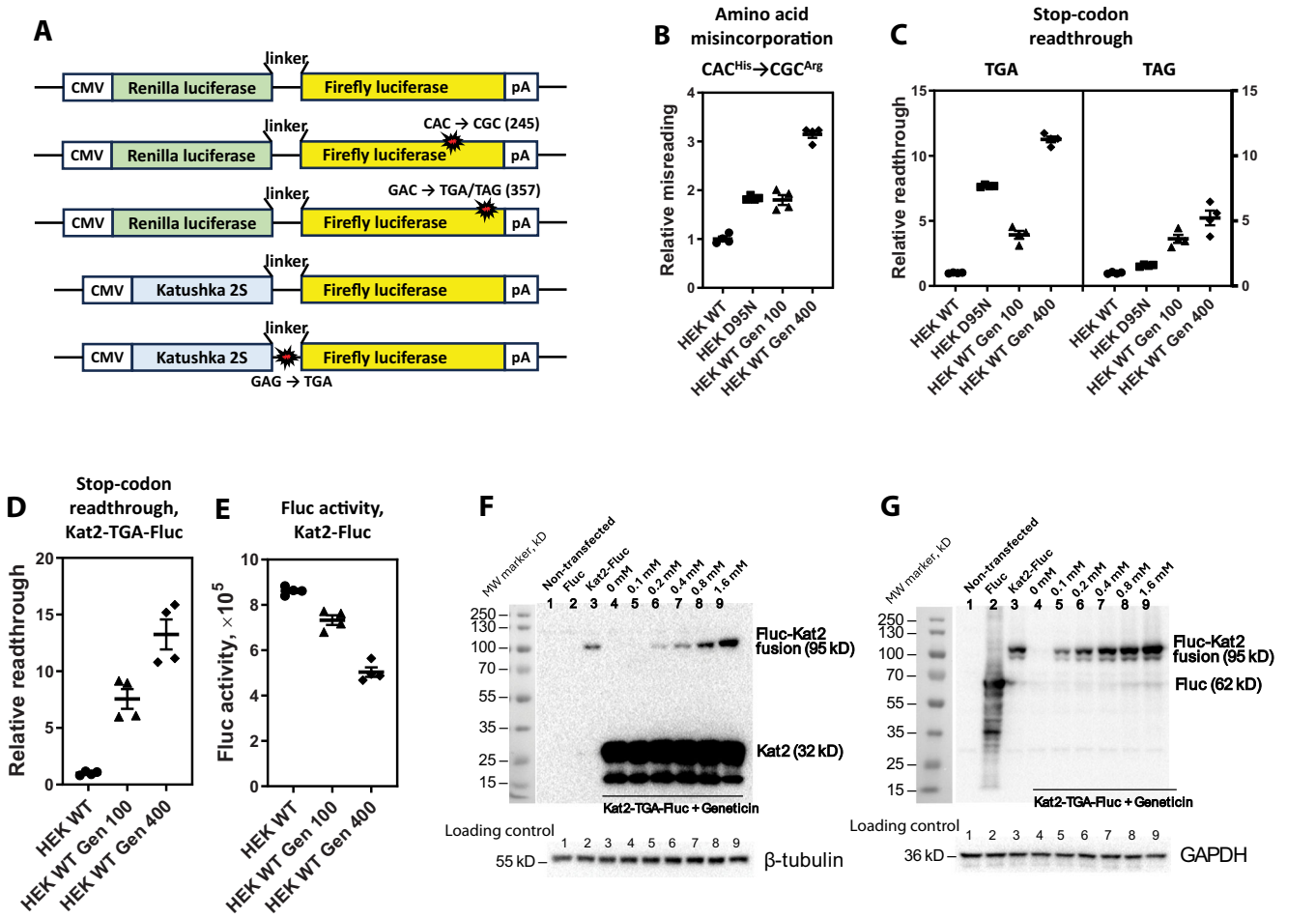

Fig. 1 | Assessment of mistranslation reporters in HEK293 cells. A Scheme of the vectors used in the experiments: Rluc-FlucWT, Rluc-Fluc^{245CGC}, Rluc-Fluc$^{357TGA/TAG}$, Kat2-Fluc, Kat2-TGA-Fluc. **B** Dual Luciferase system, misincorporation of near-cognate aa-tRNA, Rluc-Fluc^{245CGC}; **C** Dual Luciferase system, readthrough of TGA (left) and TAG (right) stop codons, Rluc-Fluc$^{357TGA/TAG}$. **D**, **E** Fluc expression relative to untreated HEK wt. **D** Kat2-TGA-Fluc construct, readthrough of TGA stop codon; **E** Kat2-Fluc construct, Fluc WT signal. **B**–**E** Data shown represent the average of three independent experiments ($N = 4$ clones each for HEK WT and HEK D95N; ± SEM). **F**, **G** WB analysis of HEK WT cells transfected with Fluc, Kat2-Fluc, or Kat2-TGA-Fluc construct and treated with increasing concentrations of geneticin, 1—HEK WT non transfected, 2—Fluc transfected 3—Kat2-Fluc transfected (no stop codon in linker as control for the molecular weight of the readthrough protein), 4–9—Kat2-TGA-Fluc transfected (stop codon in linker), 4—no geneticin, 5—0.1 mM, 6—0.2 mM, 7—0.4 mM, 8—0.8 mM, 9—1.6 mM geneticin. Antibodies against Kat2 were used in (**F**) and antibodies against Fluc were used in (**G**). β-tubulin and GABDH were used as loading control for (**F**) and (**G**) correspondingly. The experiment was repeated two times with the same results.

demonstrating that geneticin induction is dependent on the presence of a TGA stop codon (Fig. 1E). Subsequently, we performed Western blot experiments to demonstrate formation of the readthrough Kat2-Fluc fusion protein upon treatment with geneticin. As a control for the molecular weight of the readthrough protein we used HEK cells expressing Kat2-Fluc; in order not to overload the blot with an overwhelming signal we used cells transfected with low amounts of Kat2-Fluc DNA. HEK cells expressing the Kat2-Fluc construct produced a protein of 94.8 kD, corresponding to the size of the Kat2-Fluc fusion protein. Compared to cells transfected with Kat2-Fluc vector, cells transfected with Kat2-TGA-Fluc vector produced a shorter protein of 32.6kD, corresponding in size to that of Kat2 protein plus linker polypeptide (Fig. 1F). Upon treatment of Kat2-TGA-Fluc expressing cells with geneticin, we observed synthesis of a larger 94.8 kD protein in a dose-dependent manner; this protein was of identical size as the Kat2-Fluc fusion protein in Kat2-Fluc transfected cells (Fig. 1F, for mathematical calculations of geneticin-induced readthrough please see Source Data File). Fluc antibody was used to demonstrate the presence of a 3′ terminal Fluc protein in both Kat2-Fluc and in readthrough Kat2-TGA-Fluc proteins (Fig. 1G). These data demonstrate that the Kat2-TGA-Fluc construct can detect stop-codon readthrough by measurement of bioluminescence and that Fluc activity is due to formation of a readthrough protein.

Table 1 | Mistranslation frequencies in HEK293 cells

	Stop-codon readthrough (×10^{-4})		Missense miscoding (×10^{-4})
Treatment	Rluc-Fluc^{D357TGA}	Rlu-Fluc^{D357TAG}	Rluc-Fluc$^{H245R(CGC)}$
HEK293 WT	40.3 ± 1.3	18.2 ± 1.2	3.4 ± 0.3
HEK293 RPS9^{D95N}	309.3 ± 3.2	28.6 ± 1.3	6.2 ± 0.2
HEK293 WT Geneticin [100 μM]	158.2 ± 24.4	66.0 ± 11.1	6.1 ± 0.7
HEK293 WT Geneticin [400 μM]	418.3 ± 39.7	95.2 ± 20.4	10.6 ± 0.5

Generation of Kat2-TGA-Fluc mice

We generated Kat2-TGA-Fluc mice using a knock-in strategy (see Materials and Methods for details and Suppl. Figs. 2 and 3). The knock-in was performed at the *Rosa* 26 locus using the Kat2-TGA-Fluc reporter under control of the CAGGS promoter. The CAGGS promoter

https://doi.org/10.1038/s41467-025-57203-z

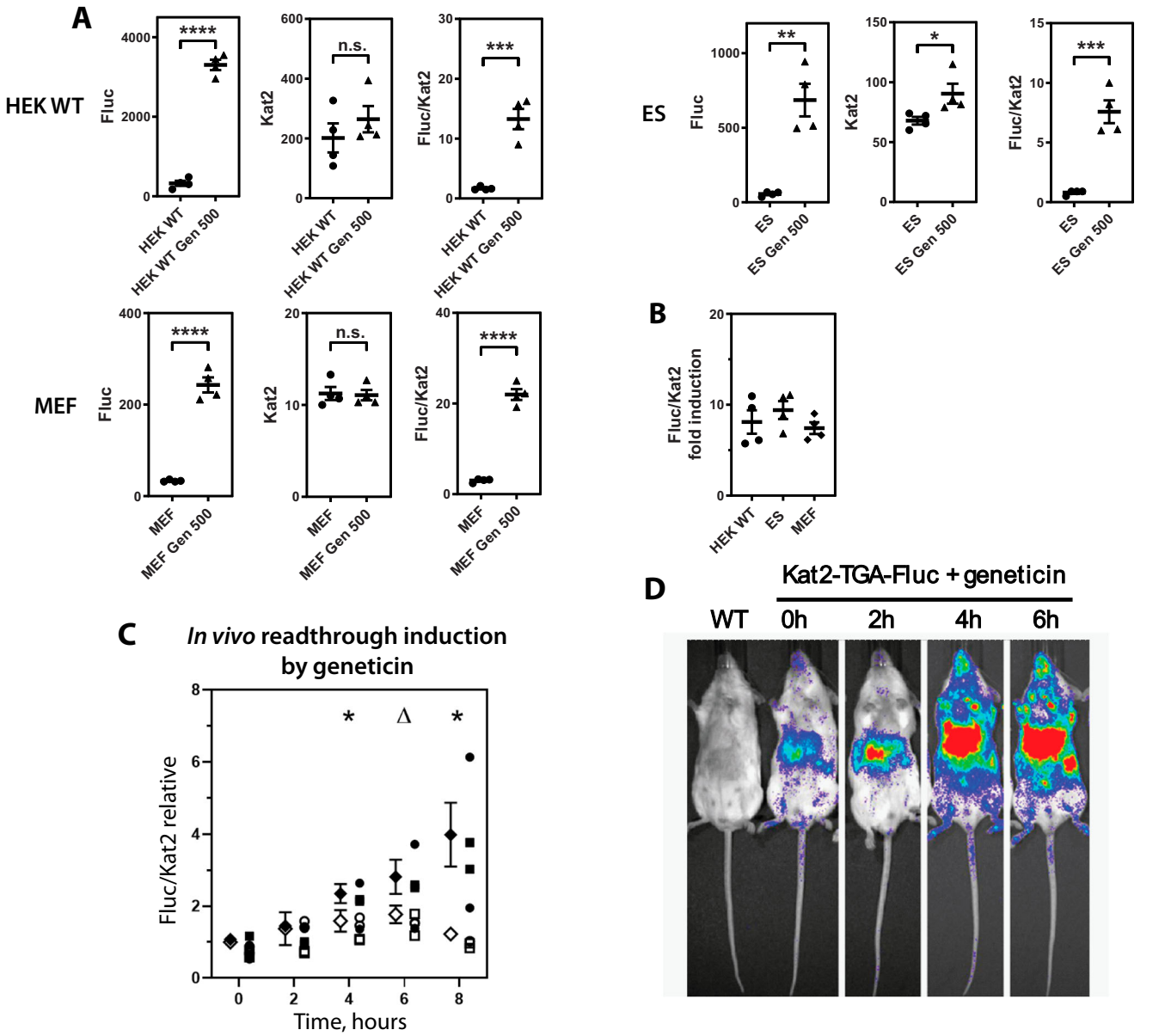

Fig. 2 | Validation of the Kat2-TGA-Fluc reporter. A Readthrough induction by geneticin in HEK293 cells (HEK WT), embryonic stem cells (ES), and murine embryonic fibroblasts (MEF) expressing the Kat2-TGA-Fluc reporter. Left graph: Fluc activity, middle graph: Kat2 activity, right graph: Fluc/Kat2 ratio. Data shown represent the average of three independent experiments using 4 clones each transfected with the corresponding reporter construct; Fluc activities (measured in relative luminescent units RLU) and Kat2 activities (measured in relative fluorescent units RFU) are shown as mean ± SEM. **B** Fold induction of readthrough activity by geneticin in HEK WT, ES, and MEF; for calculation of fold induction, the Fluc/Kat2 expression ration in untreated cells was set to 1. **C**, **D** Readthrough induction in transgenic mice expressing the Kat2-TGA-Fluc reporter following geneticin treatment (closed diamonds, $n = 4$; 2 females (closed circles), 2 males (closed squares)) in comparison to control untreated transgenic mice (open diamonds, $n = 4$; 2 females (open circles), 2 males (open squares)), ratio RLU/RFU is shown as mean ± SEM. *P* values were calculated using two-sided Student's *t*-test with equal variances. Δ $P = 0.079$, * $P \le 0.05$, ** $P \le 0.01$, *** $P \le 0.001$, **** $P \le 0.0001$, n.s. $P > 0.05$. Exact *P*-values are: (**A**) HEK WT—Fluc 8.8×10^{-7}, Kat2 3.8×10^{-1}, Fluc/Kat2 4.8×10^{-4}; ES cells—Fluc 1.2×10^{-3}, Kat2 4.5×10^{-2}, Fluc/Kat2 4.3×10^{-4}; MEF cells—Fluc 1.4×10^{-5}, Kat2 8.5×10^{-1}, Fluc/Kat2 4.6×10^{-6}; (**C**) 4.7×10^{-2} for 4 h, 7.9×10^{-2} for 6 h, 2.1×10^{-2} for 8 h.

displays ubiquitous expression including significant levels of expression in muscle and brain[47]. Recording expression of the reporter in brain and muscle is particularly relevant, as both tissues are post-mitotic tissues affected by ageing and age-related diseases.

We undertook several measures to characterize and validate the transgenic Kat2-TGA-Fluc model. First, we generated mouse embryonic fibroblasts (MEF) from the transgenic mouse line and assessed geneticin-induced expression of Fluc in MEFs, in comparison to HEK cells and embryonic stem (ES) cells expressing the Kat2-TGA-Fluc reporter (Fig. 2A). Four independently generated ES and MEF cell lines, and four independently transiently transfected batches of HEK cells expressing the Kat2-TGA-Fluc construct, were treated with 0.5 mM geneticin. Treatment with geneticin resulted in a significant induction of Fluc activity in all cells examined, with similar levels of induction of TGA codon readthrough, ranging from seven to tenfold (Fig. 2B).

Second, to address the question whether our mouse model is suitable for monitoring translational error in-vivo, we treated Kat2-TGA-Fluc mice with geneticin ($n = 8$; geneticin 2 females, 2 males; control 2 females, 2 males), a commonly used and well-established agent for in-vivo induction of translation readthrough in mice[48,49]. To record geneticin-induced readthrough, we assessed time-dependent changes in Kat2 and Fluc activity over 8 h following geneticin injection. A significant

https://doi.org/10.1038/s41467-025-57203-z

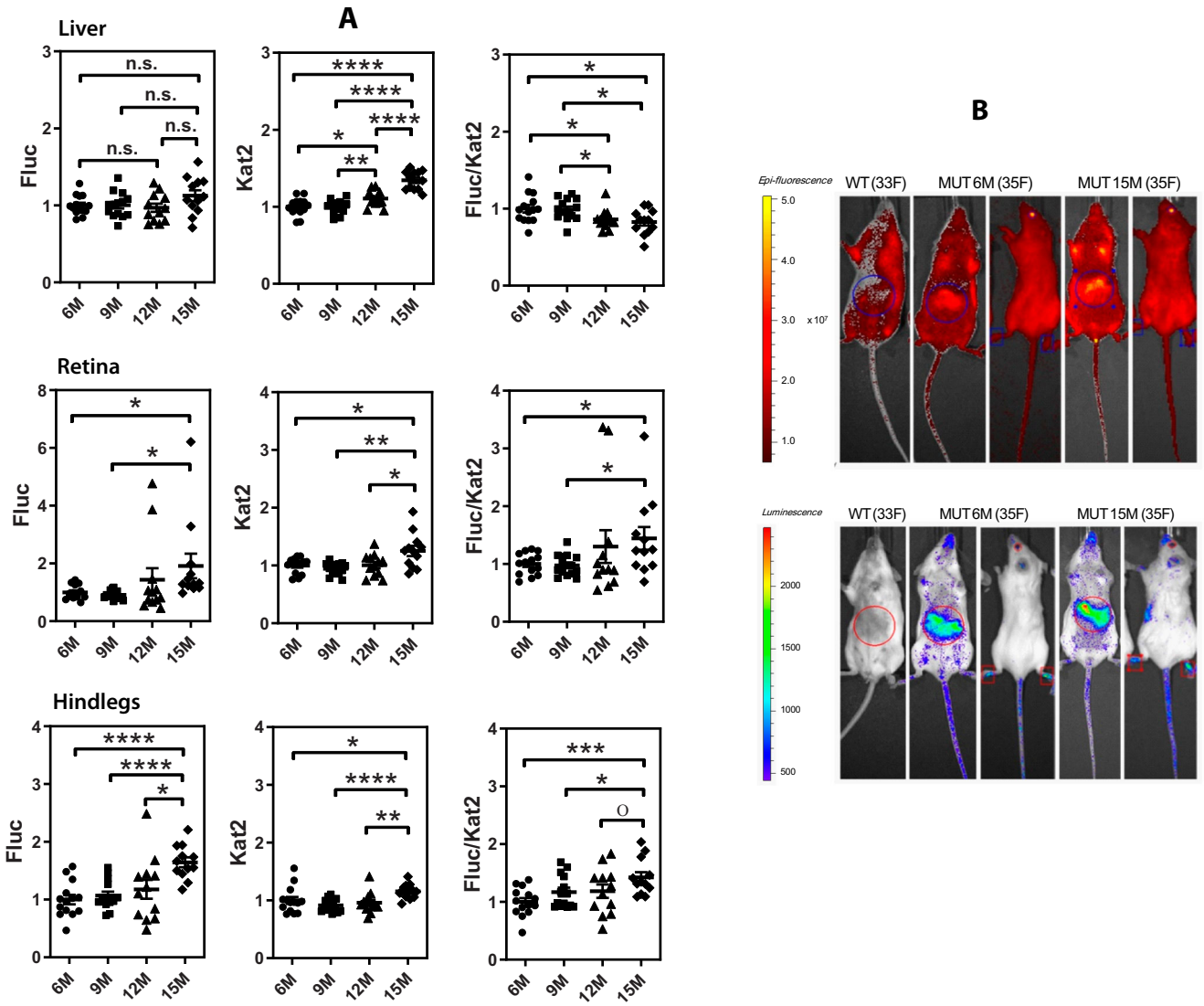

Fig. 3 | In-vivo imaging of transgenic mice expressing Kat2-TGA-Fluc construct. **A** Quantification of Luciferase (Fluc), Katushka (Kat2), and Fluc/Kat2 ratio by in-vivo imaging analysis at time points 6, 9, 12, and 15 months in liver, retina, and hindlegs; left graph: Fluc, measured in RLU, shown as mean ± SEM; middle graph: Kat2, measured in RFU, shown as mean ± SEM; right graph: Fluc/Kat2 ratio shown as mean ± SEM. Number of animals tested: for all animals $N = 14$ for 6 and 9 months, $N = 12$ for 12 and 15 months; for males $N = 6$ for 6 and 9 months, $N = 5$ for 12 and 15 months; for females $N = 8$ for 6 and 9 months, $N = 7$ for 12 and 15 months. 6 months values were set as 1. P values were calculated using two-sided Student's t-test with equal variances. o $P = 0.12$, * $P \leq 0.05$, ** $P \leq 0.01$, *** $P \leq 0.001$, **** $P \leq 0.0001$, n.s. $P > 0.05$. Exact P values are present in the Source Data File. **B** Representative images of wild type (33 F) and transgenic (35 F) female mice for in-vivo analysis of liver, retina and hindlegs at 6 months and 15 months' time points. (top) Katushka fluorescence, (bottom) Fluc luminescence. Kat2 fluorescence was measured at Ex: 605 nm, Em: 660 nm, Bin: Small, Exposure: 1 s. Fluc luminescence was measured at Bin: Small, Exposure: 5 s. Tissue-specific ROIs (Region-of-Interest) are indicated by the red edging in B; fluorescence (Kat2) and luminescence (Fluc) intensities were measured in equal areas.

time-dependent increase in Fluc and readthrough activity was observed in mice treated with geneticin but not in controls (Fig. 2C, D), without evidence for a sex-dependence of the effect. This is evidenced by Fluc/Kat2 expression ratios (Fig. 2C, time × treatment F1,28 = 25.68 $p < .0001$, time slope: geneticin +0.6903***, control ns, time × treatment × sex F1,28 = 0.6002 ns) as well as Fluc activities (Suppl. Fig. 4A, time × treatment F1,28 = 27.18 $p < .0001$, time slope: geneticin +168,600***, control ns, time × treatment × sex F1,28 = 0.5619 ns). There was no evidence for a geneticin effect in female or male mice on Kat2 activity (Suppl. Fig. 4B, time × treatment F1,28 = 1.403 ns, time slope: geneticin and control ns, time × treatment × sex F1,28 = 0.0150 ns).

In-vivo imaging

To study age-related alterations in ribosomal stop-codon readthrough, we generated a cohort of Kat2-TGA-Fluc mice to follow Kat2 and Fluc expression longitudinally over time. We assessed in-vivo bioluminescence and fluorescence activities in a non-invasive manner in male and female mice at the age of 6, 9, 12, and 15 months. We were able to record significant in-vivo reporter activities (Fig. 3A, B). However, in-vivo imaging came with some shortcomings, in particular, the lack of recordable signal in brain which resulted in the choice of retina as proxy for neuronal tissue. In addition, the presence of neighbouring tissue may compromise the reporter activities recorded, in particular for liver.

Significant increases in Fluc activity were found in retina and hindlegs at age 15 months, with variability in Fluc expression present in retina at later time points. In contrast, no age-dependent increase in Fluc activity was observed in liver and neighbouring tissue (Fig. 3A). To calculate levels of ribosomal readthrough we further normalized Fluc expression for overall reporter translation, as the Kat2 activities recorded in-vivo pointed to significant time-related changes.

https://doi.org/10.1038/s41467-025-57203-z

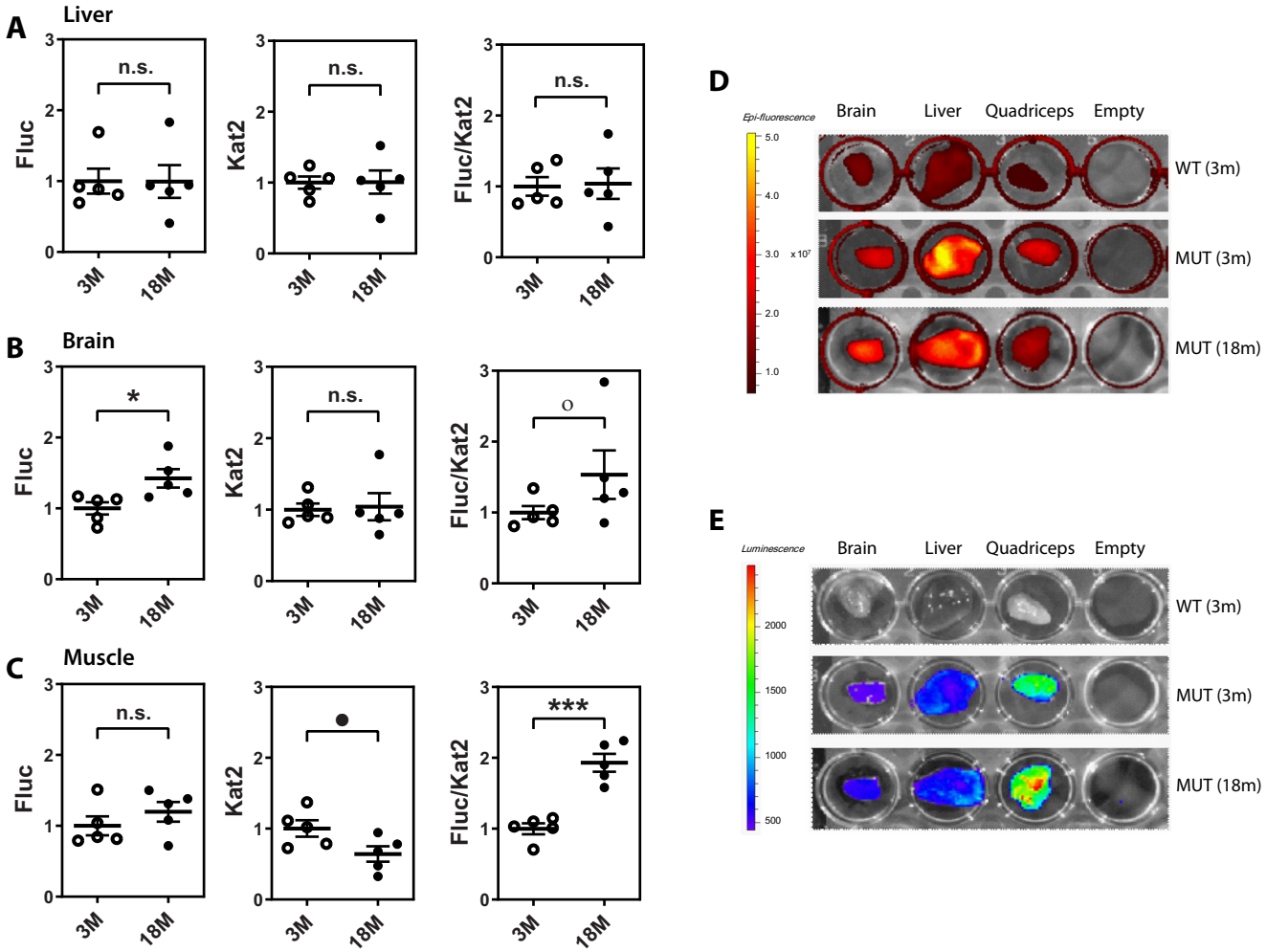

Fig. 4 | Ex-vivo imaging analysis of liver, brain, and skeletal muscle (quadriceps) from Kat2-TGA-fluc mice of 3 and 18 months of age ($N = 5$ each for 3 months and 18 months male mice). **A**–**C** Quantification of Firefly luciferase (Fluc, RLU) and Katushka 2S (Kat2, RFU) activities and calculation of Fluc/Kat2 ratio in liver (**A**), brain (**B**), and quadriceps (**C**) is shown as mean ± SEM; values are normalized to 3 months average equals 1. *P* values were calculated using two-sided Student's *t*-test with equal variances. o $P = 0.17$, ● $P = 0.055$, * $P \le 0.05$, *** $P \le 0.001$, n.s. $P > 0.05$. Exact *P*-values are: (**A**) Liver—Fluc 9.8×10^{-1}, Kat2 9.7×10^{-1}, Fluc/Kat2 8.8×10^{-1}; (**B**) Brain—Fluc 2.6×10^{-2}, Kat2 8.5×10^{-1}, Fluc/Kat2 1.7×10^{-1}; (**C**) Muscle—Fluc 3.4×10^{-1}, Kat2 5.5×10^{-2}, Fluc/Kat2 2.2×10^{-4}. **D**, **E** Representative example of fluorescent (**D**) and luminescent (**E**) comparative images of organs extracted from WT 3 months (top row), transgenic 3 months (middle row) and transgenic 18 months (bottom row) mice. The fluorescence and luminescence intensities were measured by ROI analysis in 1.6 cm^2 area for each organ.

Normalization for overall reporter translation corroborated significant age-dependent increases in ribosomal readthrough for both retina and hindlegs, as testified by a 40–45% increase in Fluc/Kat2 expression ratios at age 15 months. As expected, the lack of an age-associated increase in Fluc activity in liver came along with absence of age-related increase in ribosomal readthrough, accompanied even by decreased Fluc/Kat2 ratios. We further statistically analysed the effect of age and sex using a linear model which includes tissue and all time points as within subject factor plus sex as between subject factor. Increasing Fluc activities across ages from 6 to 15 months were found in retina and hindlegs, while no age-associated increase in Fluc activity was evident in liver (age × tissue $F2,122 = 3.948$ $p = 0.0218$, age slope: retina +0.2665**, hindleg +0.2978***, liver ns). There was no evidence for a sex effect on Fluc activity (sex $F1,10 = 2.312$ ns), nor for a sex dependency of the increases in Fluc activity in retina and hindlegs (sex × tissue × age: $F1,78 = 0.431$ ns, sex × age: retina ns, hindlegs ns). These observations were confirmed by analysis of Fluc/Kat2 expression ratios, with only retina and hindlegs showing an age-dependent increase across all ages, and liver a decrease (age × tissue $F2,122 = 10.60$ $p < .0001$, age slope: retina +0.1283*, hindleg +0.1606**, liver −0.1252***).

Ex-vivo imaging of brain, muscle, and liver

In-vivo imaging of the Kat2-TGA-Fluc mice came with limitations, in particular the inability to record suitable signals in brain, and adjacent tissue possibly affecting the measurements, namely for liver. To address these limitations, we generated a new cohort of 3 months Kat2-TGA-Fluc animals. In particular, we wished to corroborate the results from the in-vivo measurements by whole organ ex-vivo imaging of brain, muscle, and liver and to compare these animals side-by-side to transgenics of 18 months of age.

Ex-vivo imaging of isolated liver revealed no significant difference in Kat2 and Fluc activities between 3 months and 18 months animals (Kat2 $p = 0.972$, Fluc $p = 0.984$, Fig. 4A). Analysis of Kat2 and Fluc expression in brain demonstrated a significant age-associated increase in Fluc ($p = 0.026$), but not in Kat2 expression ($p = 0.85$, Fig. 4B), aligning with our results from in-vivo analysis, where we observed an age-dependent increase in Fluc activity in retina. Examination of quadriceps *ex-vivo* showed a noticeable age-associated decrease in Kat2 expression ($p = 0.055$), the marker used to normalize for overall translation of the reporter (Fig. 4C). Accordingly, we corrected the measured Fluc values for overall reporter translation by calculation of Fluc/Kat2 ratios. Calculation of quadriceps Fluc/Kat2 ratios revealed a

https://doi.org/10.1038/s41467-025-57203-z

A

	Tissue	Brain	Skeletal muscle	Liver
Fluc (RLU)	Young	1697 ± 232	22134 ± 844	7036 ± 1483
	Old	2323 ± 528	23769 ± 2040	5652 ± 1747
	P	0.041	0.136	0.214
Kat2 (RFU)	Young	32 ± 3	36 ± 5	115 ± 17
	Old	29 ± 5	23 ± 4	87 ± 10
	P	0.186	0.0012	0.013
Fluc/Kat2 (relative read-through)	Young	53 ± 11	616 ± 64	60 ± 9
	Old	80 ± 13	1074 ± 188	64 ± 20
	P	0.0075	0.00087	0.692

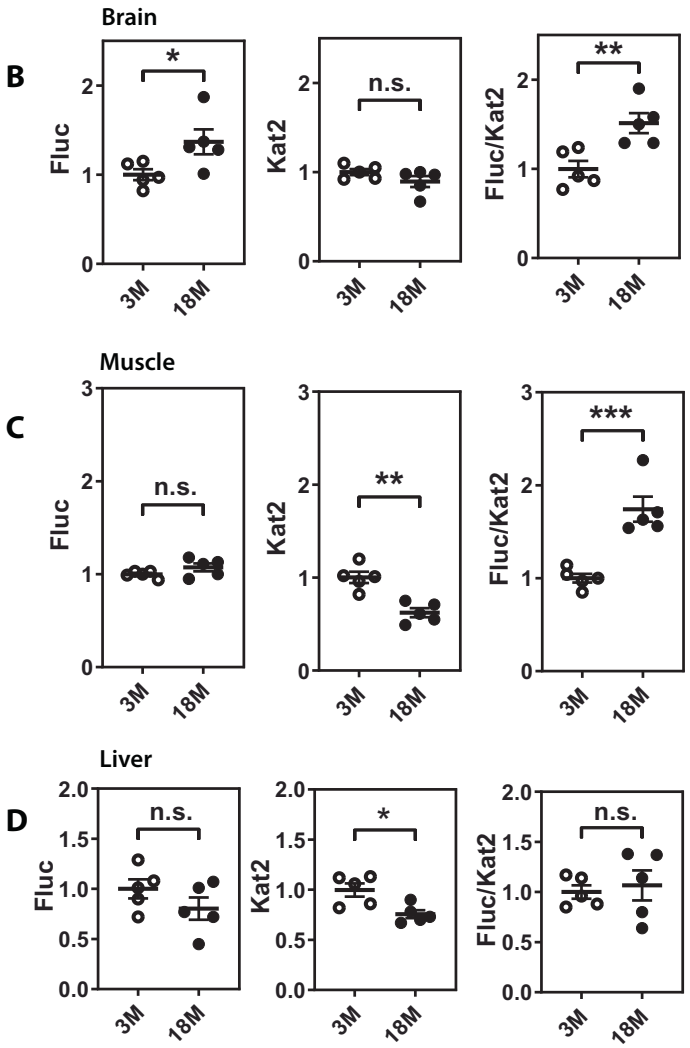

Fig. 5 | Fluc and Kat2 activities in tissue extracts from 3 and 18 months Kat2-TGA-Fluc mice. A Activities of Firefly luciferase (Fluc, RLU) and Katushka 2S (Kat2, RFU) followed by calculation of Fluc/Kat2 ratio in liver, brain and quadriceps, given as mean ± SD; $N = 5$, each for 3 months and 18 months male mice; P values were calculated using two-sided Student's t-test with equal variances. **B**–**D** Graphical representation of the data shown in (**A**). **B** brain, (**C**) muscle, (**D**) liver. Values are normalized to 3 months average equals 1. * $P \le 0.05$; ** $P \le 0.01$; *** $P \le 0.001$; n.s. $P > 0.05$; exact P-values are given in (**A**).

significant increase in ribosomal readthrough in aged 18 months animals compared to 3 months animals ($p = 0.0002$, Fig. 4C). Fluc/Kat2 ratios were also calculated for liver and brain. A mean increase in Fluc/Kat2 ratio was found in brain (+50%), although most likely due to animal variability and small sample size this was not statistically significant ($p = 0.173$). Aligning with the in-vivo data no increase in Fluc/Kat2 ratio was found for liver ($p = 0.883$).

Analysis of tissue extracts

To challenge our in-vivo and ex-vivo data which together indicate increased levels of stop-codon readthrough in brain and skeletal muscle, but not in liver, we assessed readthrough activities in-vitro in extracts from corresponding tissues of Kat2-TGA-Fluc transgenic mice. Tissue lysates from brain, skeletal muscle (quadriceps), and liver were prepared from mice 3 months and 18 months of age, Kat2 and Fluc activities determined, and readthrough values calculated by determination of Fluc/Kat2 expression ratios.

Analysis of tissue extracts corroborated the in-vivo and ex-vivo findings of an age-dependent, tissue specific increase in ribosomal readthrough (Fig. 5 and Source Data File). In detail, no age-associated increase in Fluc activity ($p > 0.05$) nor in Fluc/Kat2 expression ratio ($p > 0.05$) was observed in liver. In contrast, a significant increase in Fluc activity was found when comparing brain extracts from 3 months with 18 months animals ($p < 0.05$), this came along with an increase in relative readthrough as reflected by increased Fluc/Kat2 ratios ($p < 0.01$). As with ex-vivo analysis of quadriceps, we observed that tissue extracts from quadriceps prepared from 3 months and 18 months Kat2-TGA-Fluc mice showed a significant age-associated decrease in Kat2 expression, the marker used to calibrate overall reporter translation ($p < 0.01$). Correcting the measured Fluc values for overall reporter translation as by calculation of the Fluc/Kat2 ratios revealed significantly increased levels of readthrough in 18 months versus 3 months animals ($p < 0.001$). We used Western Blot analysis to study expression of Kat2 in muscle at the protein level. Corroborating the fluorescence data, we found that 18 months old transgenic animals showed decreased levels of Kat2 protein expression in muscle as compared to 3 months animals ($p < 0.001$, Suppl. Fig. 5C).

Together, these data demonstrate that translational readthrough increases with age in brain (+50%, $p = 0.0075$) and muscle (+75%, $p = 0,0008$), but not in liver ($p = 0.692$).

Discussion

Protein synthesis is intrinsically error-prone, leading to a constant flux of destabilized and misfolded proteins. Translational error, i.e., amino

acid misincorporation based on codon-anticodon mispairing, while rare and mostly random, is the primary limiting factor which determines the accuracy of protein synthesis. In addition to misfolding, translational errors affect the proteome and cellular fitness by various other mechanisms, such as heightened susceptibility to oxidative protein damage[50–52], ultimately leading to disruption of protein homeostasis[53,54]. The idea that translation error may be related to ageing has been an attractive and long-standing hypothesis of considerable interest. Starting with error theories of ageing back to the 1960s[55–58], early work in the 1980s investigated the question whether translational fidelity in mammalians declines with organismal or cellular ageing. These studies, in general, have not been able to detect an increase in translational errors with age, which gave rise to the perception that translational fidelity is unaffected by ageing[31,33]. However, with an average error frequency of 10^{-4} per codon[3], spontaneous misincorporations of amino acids are rare and difficult to detect. The procedures used in the 1980s to detect misincorporation of amino acids had several shortcomings, in particular these techniques were compromised by only limited sensitivity for detecting the rare translational errors[21,32]. More recent work points to translational fidelity as an important determinant of ageing. Thus, translational fidelity has been suggested to coevolve with longevity and experimentally increasing the ribosomal error rate resulted in premature ageing and shortened life span[38,40–42]. In addition, recent studies of stop-codon readthrough, a common type of translational error[3,7], indicate that this type of error may increase during aging in *Drosophila melanogaster*[39]. However, we lack any corresponding information on complex mammalian organisms, not the least due to the absence of a sensitive detection system for in-vivo recording of translational error[31,32,59].

We here have developed a highly sensitive dual reporter cassette for in-vivo assessment of translational error. We first established in human HEK cells that readthrough of stop codons is a more sensitive readout of mistranslation due to codon-anticodon mispairing than missense amino acid incorporation. Using translational stop codon readthrough as sensitive readout of mistranslation, this reporter combines a 5′ fluorescent Katushka 2S reporter with a 3′ bioluminescent Fluc reporter, separated by a stop codon containing linker which prohibits translation of Fluc. Expression of Kat2 and readthrough Kat2-Fluc proteins are under control of the same promoter, thus Kat2 activity can be used for internal normalization of overall reporter protein translation and for estimation of relative frequencies of translational errors. The luciferase-based gain-of-function assay, may in principle, detect errors in transcription, in addition to errors in translation. However, several lines of evidence argue against this possibility. In human HEK cells our mistranslation reporters show error frequencies of 3×10^{-4} (missense miscoding) and 4×10^{-3} (stop-codon readthrough), well within the range reported for translation errors[20,60,61]. With an estimated error rate of 10^{-5} to 10^{-6} per nucleotide[2] errors in transcription are about one to two orders of magnitude lower and therefore would not contribute significantly to the results. In addition, we employed two perturbations that should only affect translation: treatment with the aminoglycoside geneticin, a well-known inducer of translational misreading in eukaryotes[44], and a genetic *ram* modification conferring ribosomal mistranslation[41,62]. Both interventions significantly enhanced detected errors.

We generated transgenic mice constitutively expressing Kat2-TGA-Fluc reporter construct and validated the model using in-vivo treatment with the mistranslation-inducing agent geneticin, demonstrating significantly elevated rates of drug-induced translational readthrough. To study whether spontaneous changes in the rate of stop-codon readthrough occur as a function of age, we followed Kat2 and Fluc expression longitudinally over time in-vivo and measured expression activities at the age of 6, 9, 12, and 15 months. We were able to record significant in-vivo reporter activities. However, in-vivo imaging came with several shortcomings, e.g., lack of recordable signal in brain resulted in the choice of retina as proxy for neuronal tissue, and adjacent tissue may potentially contribute to the signal detected. In addition, despite using Kat2S as far-red fluorescent reporter with superior signal-to- noise ratio[46] and feeding mice with a chlorophyll-free diet to reduce autofluorescence, in-vivo imaging of far-red fluorescence may be hampered by tissue autofluorescence[63]. For complementing non-invasive in-vivo imaging, we generated an additional cohort of 3 months transgenic animals to allow for a direct side-by side comparison of young 3 months animals to aged 18 months transgenic mice. Considering the shortcomings of non-invasive in-vivo imaging, more refined techniques of ex-vivo analysis and defined organs and tissue extracts (liver, brain, quadriceps) were used for this analysis.

Collectively, our results from in-vivo expression studies, ex-vivo analysis of organs, and tissue extracts provide a coherent set of data, pointing to an organ-dependent, age-related increase in ribosomal error: stop-codon readthrough increased with age in muscle and brain, but not in liver. These data are at large consistent with the early in-vitro studies from the 1980s. While technical limitations at that time prevented assessments of translational fidelity in brain and muscle, studies using isolated translation competent ribosomes from rodent liver consistently failed to reveal an age-related change in ribosomal fidelity[30,64].

The experimental set-up chosen has some limitations. Firstly, we utilized stop-codon readthrough as the most sensitive proxy for codon-anticodon mispairing. Secondly, the assay does not differentiate between ribosomal and non-ribosomal mechanisms of translational fidelity. Error expression as per stop-codon readthrough reflects the assessment of the entire outcome of translation without implying a particular molecular mechanism. Thirdly, in addition to being a rare stochastic event, stop-codon readthrough may also occur in specialized systems in a non-random, programmed manner[7]. The experimental design of our study was tailored to facilitate comparison of misreading within a specific tissue over time. It is less suitable for the comparison of different tissues in-vivo, due to challenges in ensuring equal light quenching conditions and distribution of Fluc substate across the different tissues studied. Of note, Fluc is a conformationally unstable protein that requires chaperones for proper folding and enzymatic activity[65]. Given the reported age-associated decline in proteostasis capacity, as recently demonstrated in neuronal tissue[66], our estimates of age-related increases in ribosomal readthrough as per gain-of-function Fluc activity may likely be an underestimate.

Maintenance of protein homeostasis represents a formidable task because most proteins are only quasi-stable under physiologic conditions and are constantly at risk of misfolding. Cellular quality control systems safeguard protein homeostasis (proteostasis) by ensuring correct folding of new proteins, by detecting and refolding damaged proteins, and by targeting terminally misfolded proteins for degradation. Altogether, costly constant surveillance by an integrated network of chaperones and degradation machineries, comprising more than 1000 known components in the mammalian system, is required to maintain cellular proteostasis[67,68]. The collapse of proteostasis, characterized by the accumulation of misfolded and partly aggregated proteins especially in post-mitotic tissues[69,70], along with a decline in proteostasis capacity are commonly regarded as driver of cellular and organismal ageing[71–74]. The inherent inaccuracy of protein synthesis poses a challenge for protein homeostasis and represents the first and most direct process impacting on proteostasis capacity. Recently, compelling evidence has emerged demonstrating that translational accuracy affects lifespan and ageing in mammals[33,40]. In particular, it was shown that mice with increased ribosomal errors due to a knock-in *RPS9*^{D95N} *ram* mutation show premature ageing, reduced lifespan, and development of age-related disorders[40,41].

It is not clear what quantitative levels of protein synthesis error a mammalian cell can tolerate over long. The herein determined age-

related increase in stop-codon readthrough frequency we observed upon aging in muscle and brain, is in the same order of magnitude as the increase in readthrough frequency conferred by the *ram* mutation in *RPS9*^{D95N} mice[41], arguing for a pathophysiologic relevance. We emphasize that the readthrough assay we have chosen as most sensitive readout of ribosomal mistranslation due to codon-anticodon mispairing warrants future quantitative studies which directly determine missense miscoding in organismal tissue, e.g., using corresponding in-vivo reporters or high-resolution mass spectrometric analyses[6].

Our findings add to the growing perception that ribosomal fidelity is not a fixed and mere codon and sequence dependent constant, but subject to modulation by e.g., signalling pathways[75] and levels and accuracy of tRNA modifications[76]. The absolute amount of ribosomal misreading is likely to be different for different tissues. Thus, in our experiments, a direct comparison of stop-codon readthrough frequencies assessed in extracts of brain and muscle tissue from Kat2-TGA-Fluc mice points to a significantly higher readthrough frequency in muscle (Suppl. Fig. 6). While the mechanistic basis for this observation remains to be clarified and may reflect ribosomal and non-ribosomal mechanisms, such as tissue-specific limitations in tolerance to mistranslation, this finding is consistent with a previous report in transgenic mice mosaic for the strong *RPS2*^{A226V} *ram* allele, which demonstrated expression of mutant *RPS2*^{A226V} mRNA in muscle, but not in brain[42].

Aging is perceived as a general decline in cell fitness, a systems pathology affecting multiple cellular systems[77], characterized by rather slow and subtle changes in a large number of functions. At the cellular level, the reported consequences of small increases in the inherent error frequency of protein synthesis are pleiotropic and include protein misfolding and aggregation, progressive shortening of telomeres, epigenetic changes such as alterations in DNA methylation, mitochondrial dysfunction, increased production of reactive oxygen species, lipid peroxidation and oxidative protein damage[40,41,78]. It is intriguing that small changes in translational fidelity as experimentally conferred by introduction of a r*am* mutation recapitulate so many of the biochemical, cellular, and pathophysiological hallmarks attributed to ageing.

We hypothesize that in addition to an inherently error-prone protein synthesis and the reported age-related decline in proteostasis capacity[73], the age-associated increase in ribosomal error as assessed by stop-codon readthrough and herein demonstrated primarily in postmitotic tissues contributes to the overall aging process. Interestingly, this age-associated increase in ribosomal error was observed to occur in mice in late middle age, a time when physiological and behavioural signs of age-related decline begin to appear[40,41,79–81]. It will be a challenge for future studies to elucidate the mechanisms that mediate the age-related decline in translation fidelity and to pinpoint the molecular mechanisms and signal transduction pathways which translate errors in protein synthesis into ageing and age-related disease, with the view to develop therapeutic targets for the benefit of healthy ageing and amelioration of age-related diseases.

Material and methods

Construction of reporters

To study mistranslation in HEK293 cells we used vectors pRM hRluc-hFluc H245R^{CGC} and pRM hRluc-FlucD357stop$^{TGA/TAG}$ and calculated relative frequencies of near-cognate missense miscoding and stop-codon readthrough as described previously[41].

For estimation of absolute misreading frequencies, HEK293 cells were in parallel transfected with construct pRM hRluc-hFlucWT. This vector is identical to the Fluc mutant pRM vectors above but carries a WT Fluc sequence, resulting in an uninterrupted Rluc-Fluc fusion protein. Following normalization to Renilla luciferase activity, the firefly luciferase activity of the Rluc-Fluc WT vector was used for calculation of absolute misreading frequencies by dividing the Fluc activity of the mutant Fluc vectors (FlucH245R^{GCG}, FlucD357stop) by the Fluc activity of the Fluc WT vector.

For in-vivo detection of stop-codon readthrough we replaced the most part (except last 153 nucleotides) of Rluc in vector pRM hRluc-hFluc by the coding sequence of Katushka2S, resulting in vector Kat2-Fluc expressing an uninterrupted Kat2-Fluc fusion protein. A TGA stop codon was introduced into the linker identical to that from pRM hRluc-hFluc, which separates Kat2 from Fluc, resulting in the dual reporter cassette Kat2-TGA-Fluc.

Cell culture

HEK293 cells (ATCC) were cultured in Dulbecco's modified Eagle's medium (DMEM) supplemented with 10% fetal bovine serum (FBS). Generation and maintenance of HEK293 *RPS9*^{D95N} cells is described in ref. 40.

ES cells expressing the pKat2-TGA-hFluc reporter construct were cultured with MEF feeders in GMEM supplemented with 2 mM glutamine (Gibco 21710-025), 10% FBS, 1000 u/ml Leukemia inhibitor factor, 0.1 mM ß-mercaptoethanol, MEM non-essential amino acids (Gibco 11140-035), and sodium pyruvate (Gibco 11360-039). MEF cells expressing the pKat2-TGA-hFluc reporter construct were cultivated in DMEM with 10% FBS and 2 mM glutamine.

Generation of the misreading reporter mouse line

The misreading reporter mouse line was generated by knock-in strategy (genOway, France). The dual reporter cassette Kat2-TGA-Fluc containing Kat2 and Fluc coding sequences was inserted in antisense orientation at the mouse *Rosa* 26 locus. The dual reporter cassette is under the control of the CAGGS promoter (Chicken β-actin promoter coupled with cytomegalovirus (CMV) early enhancer) and terminated by the human growth hormone polyadenylation signal. Both reporters are separated by a linker containing a TGA codon to avoid Fluc expression.

The targeting vector was constructed from genomic BALB/c mouse strain DNA. A floxed Hyg^{R} (hygromycin resistance) cassette was inserted downstream of the transgene.

The linearized targeting vector was transfected into BALB/c ES cells, and positive selection was started 48 h after electroporation by addition of hygromycin B. Resistant clones were isolated, amplified, duplicated, and genotyped by both PCR and whole locus sequencing.

The following primer pairs were designed to specifically amplify the targeted locus over the long and short homology arms, respectively: 0162-ROSA: 5′- GGGCTATGAACTAATGACCCCGTAATTG-3′; 0163-ROSA: 5′- AGTGTCAAAAGACCCAACCAACAGCA-3′, and 0147-ROSA: 5′- CTTGGTGCGTTTGCGGGGAT-3′; 0034-ROSA 5′- GCAGTGAGAAGAGTACCACCATGAGTCC-3′. Proper recombination and integrity of the transgene were further confirmed by whole locus sequencing, including the expression cassette and the homology arms. PCR and sequencing led to the identification of 4 targeted clones.

Targeted ES cell clones were microinjected into C57BL/6J blastocysts and gave rise to male chimeras. Breeding with BALB/c Cre-deleter mice (CMV-Cre) led to the excision of the HygR cassette, thus producing the heterozygous Kat2-STOP-FLuc mouse line. These heterozygous animals were first identified by the following PCR primers: EBO33-29 (5′- AAGCACTTGCTCTCCCAAAGTCGC-3′) and EBO33-33 (5′- GGCTGGTCTCCAACTCCTAATCTCAGG-3′) amplifying a 702-bp fragment corresponding to the knock-in dual reporter allele devoid of Hyg^{R}, and EBO33-29 and EBO33-30 (5′- GGAAGTCTTGTCCCTCCAATTTTACACC-3′), amplifying a 325-bp fragment corresponding to the wild type allele (Suppl. Fig. 2). PCR-positive animals were further validated by whole locus sequencing, confirming the sequence integrity of the targeted locus. The line was then amplified onto BALB/c genetic background to produce experimental cohorts of heterozygous mice.

Generation of mouse embryonic fibroblasts (MEFs)

Kat2-TGA-Fluc heterozygous males were bred with wild type females. Embryos were collected at E14.5 from 2 females, dissected in PBS, and dissociated by pipetting up and down in 1-ml and then 200-µl pipette tips in Trypsin/EDTA in 24-w plates, which were then incubated at 37 °C/5% CO_2 for 5 min. Trypsin was inactivated by the addition of 1 ml MEF culture medium (Glasgow MEM medium, 10% fetal calf serum, 2.4 mM glutamine, sodium pyruvate, MEM non-essential amino acids; 120 mM beta-mercaptoethanol), and the suspension was washed once in 50 ml MEF medium by a 5′, 1250 rpm centrifugation. The pellet was resuspended in 1 ml of MEF culture medium and plated in a T75 flask for a 1-night culture in incubator. The day after dissociation, the medium was changed to remove any cell debris. MEF were cultivated for 2 days, genotyped similarly to the dual reporter mouse line (Suppl. Fig. 2C), and 1.5–2.5 million cells from passage 1 or passage 2 were frozen. Heterozygous and wild-type MEF samples were thawed prior to in vitro misreading assay. Handling and transfection of the cells are described further.

Generation of Kat2-TGA-Fluc reporter ES cell lines

Kat2-TGA-Fluc reporter ES cell lines were produced independently from the mouse model, using the same targeting vector bearing a neomycin-resistance (Neo^R) cassette instead of Hyg^R. The floxed Neo^R cassette was excised from the ES cell lines that harbor the Kat2-TGA-Fluc dual reporter cassette at the *Rosa 26* locus by Cre-mediated recombination, hence producing heterozygous dual reporter ES cell lines (Suppl. Fig. 3). Clones of interest were identified by PCR using primers EBO33-33 and EBO33-29. The primers EBO33-39 (5′- AGGC CAGAGGCCACTTGTGTAGCG-3′) and EBO33-35 (5′-CCTCTTCCCTC GTGATCTGCAACTCC-3′) amplify a 227-bp product indicative of the presence of the Neo^R cassette within the targeted allele: the absence of PCR amplification from the clones of interest validated the proper excision of the Neo^R cassette. Whole locus sequencing confirmed integrity of the dual reporter allele devoid of selection cassette. Four wild type mock clones and 4 dual reporter knock-in clones were produced. Cells were amplified and frozen (2 million cells / vial). Handling and transfection of the cells are described further.

Dual reporter mistranslation assay

Mistranslation was assessed as described previously with minor modifications[41]. In brief, missense misreading was determined using the pRM hRluc-hFluc H245R^{CGC} vector and readthrough was assessed using vectors pRM hRluc-hFluc D357stop. HEK293 cells expressing wild-type *RPS9*^{WT} or mutant *RPS9*^{D95N} were transfected using Xfect (Takara) according to the manufacturer's protocol. After 40–48-h incubation, cells were lysed, and luminescence was measured using the Cytation 5 plate reader (Bio-Tek Instruments). For geneticin treatment, cells were transfected, incubated overnight, and then treated with the drug for further 24 h before lysis and measurement of luciferase activity. For functional assays of enzymatic activity in transfected cells and studying the effects of geneticin (Figs. 1B–E and 2A), normalization was done as per using equal number of cells at the beginning of the experiment before geneticin was added. Renilla luciferase (hRluc) activity was used as internal control for normalization. Relative levels of misreading and readthrough were calculated as described[41].

To assess absolute frequencies of misreading, HEK293 WT cells were in parallel transfected with construct pRM hRluc-hFlucWT. Misreading frequencies were calculated by the ratio of hFluc^{CGC}/hRluc to hFluc^{WT}/hRluc for missense miscoding and hFluc^{TAG}/hRluc or hFluc^{TGA}/hRluc to hFluc^{WT}/hRluc for readthrough on TAG or TGA stop codons, respectively.

When using HEK293 cells, ES cells, or MEF cells expressing the Kat2-based vector pKat2-TGA-hFluc, Kat2 fluorescence was measured using the Cytation 5 plate reader (Bio-Tek Instruments) with the following filter set: excitation 588/20, emission 635/20. Relative readthrough was calculated as above. For measuring misreading, the cells were cultured in 24-well plates until reaching 50% confluence, and then treated with geneticin for an additional 24 h before lysis and measurement of luciferase and Kat2 activities.

In-vivo and ex-vivo imaging

In-vivo bioluminescence and fluorescence imaging were performed using IVIS Spectrum In-vivo Imaging System (Revvity Inc.,Waltham, MA, USA). 1 g of IVISbright D-Luciferin Potassium Salt Bioluminescent Substrate (Perkin Elmer, 122799) was dissolved into 33.3 ml PBS to give 30 mg/ml substrate solution. Mice were anesthetized with isoflurane and 150 microliters of luciferin substrate was injected subcutaneously 20 min before imaging. Mice were maintained under anaesthesia during the entire procedure from substrate injection to imaging. Luciferase luminescence was measured for 5 s with small binning. Subsequent to luciferase, the Katushka fluorescence signal was measured at Ex:605 nm, Em: 660 nm, with exposure time of 1 s and small binning.

As a positive control, mistranslation was induced in vivo by treatment with low doses of geneticin ($n = 8$; geneticin 2 females, 2 males; control 2 females, 2 males). Geneticin was dissolved in PBS to 3 mg/ml and 5 µl/g of mouse weight (e.g., 150 µl of the geneticin solution for the 30 g mouse) was injected subcutaneously immediately after 1st imaging session (time point 0). Mice were anesthetized and imaged 0, 2, 4, 6, and 8 h after geneticin injection. At time point 4 h second dosage of geneticin (1/2 of the initial dosage) was injected.

A total of 14 transgenic animals (8 females, 6 males) and 5 WT animals (3 females, 2 males) were subjected to in-vivo imaging at timepoints 6, 9, 12, and 15 months. For each time point imaging was done twice with interval of 1 week and averages were calculated. Identical regions-of-interest (ROI) were used for each tissue, respectively. In addition, a new cohort of 3 months Kat2-TGA-Fluc animals was generated to be compared side-by-side to the 18 months animals. Unexpectedly, 5/6 18 months old female mice died during the prolonged anesthesia associated with in-vivo imaging. As a result, we decided not to proceed with the in-vivo imaging for the remaining male animals, and to focus our analysis on whole organ ex-vivo imaging and analysis of tissue extracts.

For ex-vivo imaging of isolated organs, the 3 months and 18 months old male mice were sacrificed 20 min after subcutaneous injection with luciferin substrate. To minimize the time between preparation of organs and subsequent imaging and to always allow for a direct side-by-side comparison of a 3 months transgenic animal with an 18 months transgenic animal, groups of 3 mice were harvested and analysed together - a 3 months mutant, an 18 months mutant, and a WT of 3 months or 18 months of age. The organs (brain hemisphere, liver lobe, and quadriceps) were collected on ice and imaged using the IVIS Spectrum In-vivo Imaging System. Katushka fluorescence was measured at Ex:605 nm, Em: 660 nm, binning small and exposure time 5 s. Luciferase luminescence was measured for 5 min with medium binning. Empty well signals were used for normalization of fluorescent signals during different runs, and the recorded Fluc and Kat2 activities were corrected for the corresponding background activities in age-matched non-transgenic WT control animals.

Analysis of tissue extracts

Subsequent to ex-vivo imaging, the organs were shock frozen in liquid nitrogen and stored at −80 °C until further analysis.

Preparation of tissue lysates was done as described in ref. 82 with some modifications and all steps being done on ice. In brief, a piece of frozen tissue (*ca* 100 mg) was submerged in 3^X volume (for brain and muscle) or 4^X volume (for liver) of ice-cold lysis buffer containing 100 mM KPO_4 (pH 7.8), 1 mM dithiothreitol, 4 mM ethylene glycol tetraacetic acid, 4 mM EDTA, 0.7 mM PMSF, 0.5% TX-100 and immediately homogenized using plastic pestle. A small amount of alumina

(Al_2O_3 powder) was added to assist in effective tissue homogenisation. The homogenates were centrifuged at 20,000 × *g* for 15 min at 4 °C, supernatant was collected in aliquots and either shock frozen in liquid nitrogen or immediately used for Kat2 and Fluc activity measurements. Total protein concentration was determined by BCA assay (Thermo) and adjusted between samples (the final concentration was 2–5 μg/μl for the muscle and brain lysates and 5–10 μg/μl for the liver lysates).

Kat2 fluorescence and Fluc activity were measured in 96-well plates using the Cytation 5 plate reader (Bio-Tek Instruments). For Kat2 fluorescence the following filter set was used: excitation 588/20, emission 635/20. Serial twofold dilutions were prepared and used to control for the linearity of signal and to define the amount of tissue which gives the highest signal for Kat2 and Fluc while still in the linear range. Equal amounts of protein were used for analysis, adjusted to 100 μl by lysis buffer and 100 μl Fluc substrate (Promega, supplemented with ATP 0.5 mM final conc.) were added. Following subtraction of background from wild type non-transgenic animals, relative readthrough induction upon aging was calculated by the ratio of Fluc/Kat2 activity in 18 months old mice to Fluc/Kat2 activity in 3 months old mice.

Western Blot and antibodies

Total protein extracts from both HEK293 cells and mouse tissues were prepared using Urea buffer (10 mM Tris-HCl pH = 8.0, 100 mM Na_2PO_4, 8 M Urea). Protein concentration was determined using a BCA protein assay kit (Thermo), and equal amounts of protein were loaded for polyacrylamide gel electrophoresis. Following antibodies were utilized for detection: Kat2 (Invitrogen R10367), Fluc (Rockland 200-103-150, Abcam ab21176), tubulin (Abcam ab6046), and GADPH (Abcam ab9485).

Statistical analysis

Statistical analysis was performed in GraphPad Prism version 8.0.2 or Microsoft Excel. An unpaired Student's *t*-test was used to determine significant difference between analysed samples, unless otherwise specified in the figure legend.

To evaluate changes of in-vivo reporter activity with time after injection of geneticin, we used a general linear model with treatment (geneticin, control) and sex as between factors. Time (0, 2, 4, 6, 8 h post injection) was added to the model as within factor. Significant interactions were further evaluated using partial models. All calculations were done using R 4.4.1.

To evaluate changes of in-vivo reporter activity across ages, we used a general linear model with sex as between factor. Tissue (retina, hindlegs, liver) and age (6, 9, 12, 15 months) were added to the model as within factors. Skewed distributions were corrected by Box-Cox transformation. Significant interactions were further evaluated using partial models. All calculations were done using R 4.4.0.

Animal handling

Animal housing and all experimental procedures have been in accordance with the Swiss Animal Protection Law and have been approved by the Cantonal Veterinary Office of Zurich, Switzerland (licenses ZH 207/2018 and ZH 076/2023). Mice were housed in type XJ IVC cages (Allentown Inc. Allentown NJ, USA) under a 12/12-h light-dark cycle in groups of two to five, unless individual housing was required for male mice due to fighting. Feeding was ad libitum using a chlorophyl-free diet to reduce autofluorescence (Open Source Diet D10001, Research Diets Inc, New Brunswick NJ, USA).

Ethical animal research statement

All experiments performed on *M. musculus* Balb/c complied with ethical regulations for animal testing and research and were approved by the Veterinary Office of the Canton of Zurich (licenses ZH 2072018 and ZH 076/2023).

Reporting summary

Further information on research design is available in the Nature Portfolio Reporting Summary linked to this article.

Data availability

The data generated in this study are provided in the Source Data file. Source data are provided with this paper.

References

1. Loeb, L. A. & Monnat, R. J. Jr. DNA polymerases and human disease. *Nat. Rev. Genet.* **9**, 594–604 (2008).
2. Traverse, C. C. & Ochman, H. Conserved rates and patterns of transcription errors across bacterial growth states and lifestyles. *Proc. Natl. Acad. Sci. USA* **113**, 3311–3316 (2016).
3. Ogle, J. M. & Ramakrishnan, V. Structural insights into translational fidelity. *Annu. Rev. Biochem.* **74**, 129–177 (2005).
4. Gromadski, K. B. & Rodnina, M. V. Kinetic determinants of high-fidelity tRNA discrimination on the ribosome. *Mol. Cell* **13**, 191–200 (2004).
5. Wohlgemuth, I., Pohl, C., Mittelstaet, J., Konevega, A. L. & Rodnina, M. V. Evolutionary optimization of speed and accuracy of decoding on the ribosome. *Philos. Trans. R. Soc. Lond. B Biol. Sci.* **366**, 2979–2986 (2011).
6. Mordret, E. et al. Systematic detection of amino acid substitutions in proteomes reveals mechanistic basis of ribosome errors and selection for translation fidelity. *Mol. Cell* **75**, 427–441 e425 (2019).
7. Rodnina, M. V. Decoding and recoding of mRNA sequences by the ribosome. *Annu Rev. Biophys.* **52**, 161–182 (2023).
8. Kurland, C. G., Hughes, D. & Ehrenberg, M. Limitations of translational accuracy. In *Escherichia Coli and Salmonella: Cellular and Molecular Biology*. Vol. 1 (eds Neidhardt, F. C. et al.) 979–1004 (ASM Press, Washington DC, USA, 1996).
9. Zaher, H. S. & Green, R. Fidelity at the molecular level: lessons from protein synthesis. *Cell* **136**, 746–762 (2009).
10. Woese, C. R. On the evolution of the genetic code. *Proc. Natl. Acad. Sci. USA* **54**, 1546–1552 (1965).
11. Roy, B., Leszyk, J. D., Mangus, D. A. & Jacobson, A. Nonsense suppression by near-cognate tRNAs employs alternative base pairing at codon positions 1 and 3. *Proc. Natl. Acad. Sci. USA* **112**, 3038–3043 (2015).
12. Muramatsu, T. et al. Codon and amino-acid specificities of a transfer RNA are both converted by a single post-transcriptional modification. *Nature* **336**, 179–181 (1988).
13. Nedialkova, D. D. & Leidel, S. A. Optimization of codon translation rates via tRNA modifications maintains proteome integrity. *Cell* **161**, 1606–1618 (2015).
14. Schosserer, M. et al. Methylation of ribosomal RNA by NSUN5 is a conserved mechanism modulating organismal lifespan. *Nat. Commun.* **6**, 6158 (2015).
15. Sloan, K. E. et al. Tuning the ribosome: the influence of rRNA modification on eukaryotic ribosome biogenesis and function. *RNA Biol.* **14**, 1138–1152 (2017).
16. Suzuki, T. The expanding world of tRNA modifications and their disease relevance. *Nat. Rev. Mol. Cell Biol.* **22**, 375–392 (2021).
17. Al-Hadid, Q., Roy, K., Chanfreau, G. & Clarke, S. G. Methylation of yeast ribosomal protein Rpl3 promotes translational elongation fidelity. *RNA* **22**, 489–498 (2016).
18. Shin, B. S. et al. eEF2 diphthamide modification restrains spurious frameshifting to maintain translational fidelity. *Nucleic Acids Res.* **51**, 6899–6913 (2023).
19. Kramer, E. B. & Farabaugh, P. J. The frequency of translational misreading errors in E. coli is largely determined by tRNA competition. *RNA* **13**, 87–96 (2007).

20. Kramer, E. B., Vallabhaneni, H., Mayer, L. M. & Farabaugh, P. J. A comprehensive analysis of translational missense errors in the yeast Saccharomyces cerevisiae. *RNA* **16**, 1797–1808 (2010).
21. Luce, M. C. & Bunn, C. L. Decreased accuracy of protein synthesis in extracts from aging human diploid fibroblasts. *Exp. Gerontol.* **24**, 113–125 (1989).
22. Wilson, D. L., Hall, M. E. & Stone, G. C. Test of some aging hypotheses using two-dimensional protein mapping. *Gerontology* **24**, 426–433 (1978).
23. Harley, C. B., Pollard, J. W., Chamberlain, J. W., Stanners, C. P. & Goldstein, S. Protein synthetic errors do not increase during aging of cultured human fibroblasts. *Proc. Natl. Acad. Sci. USA* **77**, 1885–1889 (1980).
24. Wojtyk, R. I. & Goldstein, S. Fidelity of protein synthesis does not decline during aging of cultured human fibroblasts. *J. Cell Physiol.* **103**, 299–303 (1980).
25. Laughrea, M. On the error theories of aging. A review of the experimental data. *Exp. Gerontol.* **17**, 305–317 (1982).
26. Pollard, J. W., Harley, C. B., Chamberlain, J. W., Goldstein, S. & Stanners, C. P. Is transformation associated with an increased error frequency in mammalian cells? *J. Biol. Chem.* **257**, 5977–5979 (1982).
27. Mori, N., Hiruta, K., Funatsu, Y. & Goto, S. Codon recognition fidelity of ribosomes at the first and second positions does not decrease during aging. *Mech. Ageing Dev.* **22**, 1–10 (1983).
28. Szajnert, M. F. & Schapira, F. Properties of purified tyrosine aminotransferase from adult and senescent rat liver. *Gerontology* **29**, 311–319 (1983).
29. Filion, A. M. & Laughrea, M. Translation fidelity in the aging mammal: studies with an accurate in vitro system on aged rats. *Mech. Ageing Dev.* **29**, 125–142 (1985).
30. Laughrea, M. & Latulippe, J. The poly(U) translational capacity of Fischer 344 rat liver does not deteriorate with age and is not affected by dietary regime. *Mech. Ageing Dev.* **45**, 137–143 (1988).
31. Anisimova, A. S., Alexandrov, A. I., Makarova, N. E., Gladyshev, V. N. & Dmitriev, S. E. Protein synthesis and quality control in aging. *Aging (Albany NY)* **10**, 4269–4288 (2018).
32. Rattan, S. I. Synthesis, modifications, and turnover of proteins during aging. *Exp. Gerontol.* **31**, 33–47 (1996).
33. Ke, Z., Seluanov, A. & Gorbunova, V. Accurate translation is important for longevity. *Aging (Albany NY)* **10**, 297–298 (2018).
34. Anisimova, A. S. et al. Multifaceted deregulation of gene expression and protein synthesis with age. *Proc. Natl. Acad. Sci. USA* **117**, 15581–15590 (2020).
35. Kelmer Sacramento, E. et al. Reduced proteasome activity in the aging brain results in ribosome stoichiometry loss and aggregation. *Mol. Syst. Biol.* **16**, e9596 (2020).
36. Gerashchenko, M. V., Peterfi, Z., Yim, S. H. & Gladyshev, V. N. Translation elongation rate varies among organs and decreases with age. *Nucleic Acids Res.* **49**, e9 (2021).
37. Llewellyn, J., Hubbard, S. J. & Swift, J. Translation is an emerging constraint on protein homeostasis in ageing. *Trends Cell Biol.* **34**, 646–656 (2024).
38. Ke, Z. et al. Translation fidelity coevolves with longevity. *Aging Cell* **16**, 988–993 (2017).
39. Martinez-Miguel, V. E. et al. Increased fidelity of protein synthesis extends lifespan. *Cell Metab.* **33**, 2288–2300 e2212 (2021).
40. Brilkova, M. et al. Error-prone protein synthesis recapitulates early symptoms of Alzheimer disease in aging mice. *Cell Rep.* **40**, 111433 (2022).
41. Shcherbakov, D. et al. Premature aging in mice with error-prone protein synthesis. *Sci. Adv.* **8**, eabl9051 (2022).
42. Moore, J. et al. Random errors in protein synthesis activate an age-dependent program of muscle atrophy in mice. *Commun. Biol.* **4**, 703 (2021).
43. Matt, T. et al. Dissociation of antibacterial activity and aminoglycoside ototoxicity in the 4-monosubstituted 2-deoxystreptamine apramycin. *Proc. Natl. Acad. Sci. USA* **109**, 10984–10989 (2012).
44. Oishi, N. et al. XBP1 mitigates aminoglycoside-induced endoplasmic reticulum stress and neuronal cell death. *Cell Death Dis.* **6**, e1763 (2015).
45. Mezzanotte, L., Blankevoort, V., Lowik, C. W. & Kaijzel, E. L. A novel luciferase fusion protein for highly sensitive optical imaging: from single-cell analysis to in vivo whole-body bioluminescence imaging. *Anal. Bioanal. Chem.* **406**, 5727–5734 (2014).
46. Luker, K. E. et al. Comparative study reveals better far-red fluorescent protein for whole body imaging. *Sci. Rep.* **5**, 10332 (2015).
47. Tchorz, J. S. et al. A modified RMCE-compatible Rosa26 locus for the expression of transgenes from exogenous promoters. *PLoS ONE* **7**, e30011 (2012).
48. Yang, C. et al. A mouse model for nonsense mutation bypass therapy shows a dramatic multiday response to geneticin. *Proc. Natl. Acad. Sci. USA* **104**, 15394–15399 (2007).
49. Heier, C. R. & DiDonato, C. J. Translational readthrough by the aminoglycoside geneticin (G418) modulates SMN stability in vitro and improves motor function in SMA mice in vivo. *Hum. Mol. Genet.* **18**, 1310–1322 (2009).
50. Stadtman, E. R. Protein oxidation and aging. *Science* **257**, 1220–1224 (1992).
51. Dukan, S. et al. Protein oxidation in response to increased transcriptional or translational errors. *Proc. Natl. Acad. Sci. USA* **97**, 5746–5749 (2000).
52. Krisko, A. & Radman, M. Phenotypic and genetic consequences of protein damage. *PLoS Genet.* **9**, e1003810 (2013).
53. Drummond, D. A. & Wilke, C. O. Mistranslation-induced protein misfolding as a dominant constraint on coding-sequence evolution. *Cell* **134**, 341–352 (2008).
54. Powers, E. T. & Balch, W. E. Costly mistakes: translational infidelity and protein homeostasis. *Cell* **134**, 204–206 (2008).
55. Medvedev, Z. [Aging of the body on the molecular level]. *Usp. Sovrem. Biol.* **51**, 299–316 (1961).
56. Orgel, L. E. The maintenance of the accuracy of protein synthesis and its relevance to ageing. *Proc. Natl. Acad. Sci. USA* **49**, 517–521 (1963).
57. Orgel, L. E. The maintenance of the accuracy of protein synthesis and its relevance to ageing: a correction. *Proc. Natl. Acad. Sci. USA* **67**, 1476 (1970).
58. Edelmann, P. & Gallant, J. On the translational error theory of aging. *Proc. Natl. Acad. Sci. USA* **74**, 3396–3398 (1977).
59. Iben, S. To aggregate or not to aggregate - Is it a matter of the ribosome? *Bioessays* **45**, e2200230 (2023).
60. Namy, O., Duchateau-Nguyen, G. & Rousset, J. P. Translational readthrough of the PDE2 stop codon modulates cAMP levels in Saccharomyces cerevisiae. *Mol. Microbiol.* **43**, 641–652 (2002).
61. Dunn, J. G., Foo, C. K., Belletier, N. G., Gavis, E. R. & Weissman, J. S. Ribosome profiling reveals pervasive and regulated stop codon readthrough in Drosophila melanogaster. *Elife* **2**, e01179 (2013).
62. Zaher, H. S. & Green, R. Hyperaccurate and error-prone ribosomes exploit distinct mechanisms during tRNA selection. *Mol. Cell* **39**, 110–120 (2010).
63. Lifante, J., Shen, Y. L., Ximendes, E., Rodríguez, E. M. & Ortgies, D. H. The role of tissue fluorescence in optical bioimaging. *J. Appl. Phys.* **128**, 171101 (2020).
64. Butzow, J. J., McCool, M. G. & Eichhorn, G. L. Does the capacity of ribosomes to control translation fidelity change with age? *Mech. Ageing Dev.* **15**, 203–216 (1981).

65. Gupta, R. et al. Firefly luciferase mutants as sensors of proteome stress. *Nat. Methods* **8**, 879–884 (2011).
66. Blumenstock, S. et al. Fluc-EGFP reporter mice reveal differential alterations of neuronal proteostasis in aging and disease. *EMBO J.* **40**, e107260 (2021).
67. Balch, W. E., Morimoto, R. I., Dillin, A. & Kelly, J. W. Adapting proteostasis for disease intervention. *Science* **319**, 916–919 (2008).
68. Hipp, M. S., Park, S. H. & Hartl, F. U. Proteostasis impairment in protein-misfolding and -aggregation diseases. *Trends Cell Biol.* **24**, 506–514 (2014).
69. Lindner, A. B. & Demarez, A. Protein aggregation as a paradigm of aging. *Biochim. Biophys. Acta* **1790**, 980–996 (2009).
70. Cuanalo-Contreras, K. et al. Extensive accumulation of misfolded protein aggregates during natural aging and senescence. *Front. Aging Neurosci.* **14**, 1090109 (2022).
71. Taylor, R. C. & Dillin, A. Aging as an event of proteostasis collapse. *Cold Spring Harb. Perspect. Biol*. **3** https://doi.org/10.1101/cshperspect.a004440 (2011).
72. Labbadia, J. & Morimoto, R. I. The biology of proteostasis in aging and disease. *Annu. Rev. Biochem.* **84**, 435–464 (2015).
73. Hipp, M. S., Kasturi, P. & Hartl, F. U. The proteostasis network and its decline in ageing. *Nat. Rev. Mol. Cell Biol*. **20**, 421–435 (2019).
74. Santra, M., Dill, K. A. & de Graff, A. M. R. Proteostasis collapse is a driver of cell aging and death. *Proc. Natl. Acad. Sci. USA* **116**, 22173–22178 (2019).
75. Conn, C. S. & Qian, S. B. Nutrient signaling in protein homeostasis: an increase in quantity at the expense of quality. *Sci. Signal* **6**, ra24 (2013).
76. Huber, S. M. et al. Arsenite toxicity is regulated by queuine availability and oxidation-induced reprogramming of the human tRNA epitranscriptome. *Proc. Natl. Acad. Sci. USA* **119**, e2123529119 (2022).
77. Lopez-Otin, C., Blasco, M. A., Partridge, L., Serrano, M. & Kroemer, G. Hallmarks of aging: an expanding universe. *Cell* **186**, 243–278 (2023).
78. Shcherbakov, D. et al. Ribosomal mistranslation leads to silencing of the unfolded protein response and increased mitochondrial biogenesis. *Commun. Biol.* **2**, 381 (2019).
79. Prenderville, J. A., Kennedy, P. J., Dinan, T. G. & Cryan, J. F. Adding fuel to the fire: the impact of stress on the ageing brain. *Trends Neurosci.* **38**, 13–25 (2015).
80. Clayton, Z. S. et al. Lifelong physical activity attenuates age- and Western-style diet-related declines in physical function and adverse changes in skeletal muscle mass and inflammation. *Exp. Gerontol.* **157**, 111632 (2022).
81. Murray, K. O. et al. The plasma metabolome is associated with preservation of physiological function following lifelong aerobic exercise in mice. *Geroscience* **46**, 3311–3324 (2024).
82. Goeman, F. et al. Molecular imaging of nuclear factor-Y transcriptional activity maps proliferation sites in live animals. *Mol. Biol. Cell* **23**, 1467–1474 (2012).

Acknowledgements

We thank Sonia Matos for help with the issue work up and Markus Rudin for help in design of the Kat2-Fluc reporter. This study was supported in part by the University of Zurich.

Author contributions

Concept of study: E.C.B., R.A., and D.S. Supervision of study: E.C.B. Design and testing of reporters: R.A. and D.S. Construction of transgenic mice: E.S., K.T., and P.I. Animal handling: A.S., H.S.K., P.S., and D.W. In-vivo imaging: H.S.K., R.A., and A.S. Ex-vivo imaging: H.S.K. and R.A. Tissue work up: D.S. Analysis of tissues: D.S. and R.A. Statistical analysis: R.A., D.S., D.W., and H.S.K. All authors analysed and discussed the data E.C.B., D.S., and R.A. wrote the paper with input from all authors

Competing interests

We declare that none of the authors have competing financial or non-financial interests as defined by Nature Portfolio.

Additional information

Supplementary information The online version contains supplementary material available at https://doi.org/10.1038/s41467-025-57203-z.

Correspondence and requests for materials should be addressed to Rashid Akbergenov.

Peer review information *Nature Communications* thanks the anonymous reviewer(s) for their contribution to the peer review of this work. A peer review file is available.